Title: Ultrastructural and transcriptional profiling of neuropathological misregulation of CREB function

Running title: Misregulation of CREB function

Authors and affiliations: [1] Luis M Valor, [1] Dragana Jancic, [2] Rafael Lujan and [1] Angel Barco

[1] Instituto de Neurociencias de Alicante (Universidad Miguel Hernández-Consejo Superior de Investigaciones Científicas). Campus de Sant Joan. Apt. 18. Sant Joan d'Alacant. 03550. Alicante, Spain

[2] Departamento de Ciencias Médicas. Facultad de Medicina and Centro Regional de Investigaciones Biomédicas. Universidad Castilla-La Mancha, Campus Biosanitario, C/Almansa 14, 02006, Albacete, Spain

Corresponding authors: Angel Barco, Instituto de Neurociencias de Alicante (UMH-CSIC), Campus de Sant Joan, Apt. 18, Sant Joan d'Alacant 03550, Alicante, Spain. Phone: +34 965 919232. Fax: +34 965 919492. Email: abarco@umh.es. Luis M Valor, Instituto de Neurociencias de Alicante (UMH-CSIC), Campus de Sant Joan, Apt. 18, Sant Joan d'Alacant 03550, Alicante, Spain. Phone: +34 965 919531. Fax: +34 965 919492. Email: lmv@umh.es

ABSTRACT

We compare here the neurodegenerative processes observed in the hippocampus of bitransgenic mice with chronically altered levels of CREB function. The combination of genome-wide transcriptional profiling of degenerating hippocampal tissue with microscopy analyses reveals that the sustained inhibition of CREB function in A-CREB mice is associated with dark neuron degeneration, whereas its strong chronic activation in VP16-CREB mice primarily causes excitotoxic cell death and inflammation. Furthermore, the meta-analysis with gene expression profiles available in public databases identifies relevant common markers to other neurodegenerative processes and highlights the importance of the immune response in neurodegeneration. Overall, these analyses define the ultrastructural and transcriptional signatures associated with these two forms of hippocampal neurodegeneration, confirm the importance of fine-tuned regulation of CREB-dependent gene expression for CA1 neuron survival and function, and provide novel insight into the role of CREB in the etiology of neurodegenerative processes.

Keywords: cAMP pathway, neurodegeneration, excitotoxicity, apoptosis, inflammation

INTRODUCTION

The cAMP signaling pathway is activated in neurons in response to a wide array of stimuli. Synaptic activity, hormones, growth factors released during development, hypoxia, and stress, among other stimuli, can trigger the phosphorylation of the cAMP-response element binding protein (CREB), causing its activation and the subsequent induction of a transient wave of CREB-dependent gene expression (1). This activity is necessary for the survival of different neuronal subtypes both *in vitro* and *in vivo* (2-6). The requirement for CREB is very stringent in the peripheral nervous system (7), whereas in the central nervous system, most neuronal types are only affected when both CREB and the cAMP-response element modulator (CREM) are eliminated or inhibited (8-10).

Our previous research on bitransgenic mice expressing either a strong dominant negative CREB/CREM inhibitor (A-CREB) or a constitutively active CREB variant (VP16-CREB) revealed markedly different initial effects of repressing or boosting the CREB activity in neuronal gene expression and physiology. A-CREB reduced intrinsic excitability and impaired long-term potentiation (LTP) (10), whereas VP16-CREB enhanced excitability (11) and LTP (12). Strikingly, these divergent early effects led to apparently similar late deleterious effects, since both manipulations caused in the long-term a severe loss of neurons in the CA1 subfield of the hippocampus in a dose and time dependent manner (10, 11).

Do both the blockade and the enhancement of CREB function trigger the same cell death program? Is CREB misregulation, as previously proposed (13-18), involved in neurodegenerative diseases? To answer these questions, we performed parallel histological and cell death assays as well as gene profiling in the hippocampus of A-CREB and VP16-CREB mice. We define the ultrastructural the transcriptional

signatures associated with these two forms of neurodegeneration, and show that a sustained blockade of CREB function leads to atrophy and dark neuron degeneration, whereas its strong chronic activation eventually causes excitotoxic cell death and widespread inflammation. These two processes are associated with differential activation of the immune response that determines the extent of the neuronal damage.

RESULTS

Chronic inhibition of CREB function causes dark neuron degeneration

We used electron microscopy analysis to investigate the mechanism of cell death underlying the shrinkage of the CA1 subfield observed in brain sections of bitransgenic mice expressing the strong inhibitor of the CREB family of transcription factors A-CREB for several weeks (10). The CA1 pyramidal cell layer of six-week old A-CREB mice, a time in which the loss of CA1 neurons started to become evident by Nissl staining, contained a large number of shrunken pyramidal cells with highly osmiophilic cytoplasm (Fig. 1). These heteropycnotic cells, which represented up to 20% of the pyramidal neurons in the dorsal hippocampus of A-CREB mice (inset in Fig. 1B), showed apparent nuclear and cytoplasmic condensation, clumping of chromatin and their nuclear and plasma membranes were ruffled (Fig. 1C). Although most subcellular organelles appeared to be normal, some cells exhibited swelling of mitochondria and the Golgi network. There was no fragmentation of the nucleus or cytoplasm, and adjacent neurons had a normal appearance. This description fits with what has been referred to as dark cell or dark neuron degeneration, a form of neuronal death some times associated with positive TUNEL staining, a common marker of apoptotic cell death (19, 20). In fact, the analysis of brain sections from A-CREB mice revealed the presence of TUNEL positive neurons in the CA1 subfield preceding

the spread of cell loss in this area (Fig. 1D). At later times, when the thickness of the cellular layer was severely reduced and there were few cells positive for transgene expression, we did not observe cells positive for TUNEL staining (bottom panel). In agreement with these results, we also found neurons positive for active caspase-3, another marker of apoptotic cell death, in the sections from 6-week old A-CREB mice (Sup. Fig. S1A). Brain sections of A-CREB mice were also positive for a reduced-silver staining that labels degenerating neurons (Sup. Fig. S1B). These results, together with the reduced excitability and impaired plasticity observed in previous electrophysiological analyses (10), suggest that reduced responsiveness in A-CREB expressing neurons may lead to the activation of an apoptotic program that eliminates transgene expressing cells, explaining both the shrinkage of the cellular layer at the CA1 subfield and the loss of transgene expression in old mice.

Chronic enhancement of CREB function causes inflammation

Previous studies have demonstrated that bitransgenic mice expressing a constitutively active CREB variant at a high level (VP16-CREB^{high}) showed enhanced intrinsic excitability and synaptic plasticity in the hippocampus shortly after transgene induction (11, 12), but late spontaneous seizures and a loss of CA1 pyramidal neurons (11). In agreement with these results, the electron microscopy analysis of VP16-CREB^{high} mice showed that the pyramidal cell layer maintained a normal appearance during the first two weeks after transgene induction (Fig. 2A, F-I). However, three weeks after transgene induction, incipient local signs of neurodegeneration were observed. Infiltrated glial cells, some cell debris, and vacuolated neurons were observed between the cell bodies of apparently intact CA1 pyramidal neurons (Fig. 2B, D). Six weeks after dox removal, the number of pyramidal neurons was severely reduced and massive astrogliosis was apparent in both the cellular and the dendritic

layer (Fig. 2C, E). The immunohistological analysis using antibodies against the astrocyte marker GFAP (Fig. 3A) and the activated microglia marker F4/80 (Fig. 3B) confirmed the active gliosis observed in the electron microscopy images.

In terms of the number and morphology of synapses in the *stratum radiatum*, we did not observe significant differences two weeks after induction in either inhibitory or excitatory synapses (Fig. 2F-I). However, there was a pronounced reduction of glutamatergic synapses in mice expressing the transgene for six weeks (Fig. 2M: wt: 166±4 syn/100mm^3; VP16-CREB^{high}: 27±2 syn/100mm^3; $p<0.001$). At these late times, we also observed ultrastructural abnormalities both at postsynaptic and presynaptic sites. Dendritic spines appeared smaller and elongated, whereas axonal terminals were enlarged and contained fewer synaptic vesicles and mitochondria (Fig. 2J-L).

Although it is now believed that seizure-induced neuronal death is primarily morphologically necrotic, excitotoxic insults result in mixed apoptotic-necrotic features depending on their intensity (20, 21). Consistent with this view, we found cells positive for TUNEL reaction in the hippocampus of VP16-CREB^{high} mice three weeks after induction (Fig. 2N). Brain sections obtained at either earlier (one to two weeks) or later (six or more weeks) times after transgene induction were negative for this assay. The brain sections of VP16-CREB^{high} mice were also positive for silver staining, (Sup. Fig. S1B). Neither cell loss nor TUNEL or neurosilver positive neurons were observed in bitransgenic mice that expresses lower levels of VP16-CREB protein (VP16-CREB^{low}), even after one year of transgene expression (results not shown).

The features of degenerating neurons in VP16-CREB^{high} mice, together with the enhanced excitability of VP16-CREB expressing neurons and the spontaneous

epileptic activity (11), indicate that cellular loss in the hippocampus of these mice is primarily caused by excitotoxic neuronal death and includes degenerating neurons undergoing apoptotic cell death. Notably, the inflammatory process associated to strong chronic activation of the CREB pathway was absent or very minor in mice with reduced CREB function: GFAP immunoreactivity was stronger and more widespread in the hippocampus of VP16-CREB^{high} mice than in A-CREB mice (Fig. 3A), and reactive microglia was detected only in the former (Fig. 3B). These observations were confirmed by gene expression analysis (Figs. 4G, S3 and Supplemental Tables 1 and 2).

Gene expression profiles of chronic inhibition or enhancement of CREB function

To gain additional insight into the pathological processes triggered by abnormal activity in the CREB pathway, we investigated the gene expression profiles active during ongoing neurodegeneration using microarrays. RNA samples from bitransgenic mice at the onset of neurodegeneration (i.e., six-week old A-CREB mice and VP16-CREB^{high} mice three weeks after transgene induction, referred to as A-CREB and VP16-CREB late samples, respectively) were compared with those from their respective control littermates. For comparison purposes, we also examined samples obtained at earlier time points of transgene expression, in which there were no evident signs of neuronal death (three-week old A-CREB mice and VP16-CREB^{high} mice one week after transgene induction, referred as A-CREB early and VP16-CREB early, respectively).

As expected for an activity-regulated transcription factor, CREB inhibition had a milder effect on basal gene expression than its overactivation both at early (51 *vs.* 280 probe sets) and late times (62 *vs.* 1566 probe sets) of transgene expression

(Fig. 4A and Sup. Tables 1 and 2). We found that at early times gene downregulations prevailed, although not significantly, in A-CREB mice (60.8%, P = 0.32, Fisher's exact test), whereas upregulations were more frequent in VP16-CREB mice (85.4%, $P = 1.66 \times 10^{-19}$). To some extent, these numbers are in agreement with the expected effect of a dominant negative and a constitutively active form of a transcription factor. In contrast, at later times, we observed a dramatic increase in the number of upregulated probe sets in A-CREB mice (39.2% in early samples compared to 95.2% in late samples, $P = 4 \times 10^{-11}$) and the activation of a broad genetic program (>1000 genes) in VP16-CREB mice that included a large number of downregulated genes (41 probe sets in early samples compared to 336 probe sets in late samples, P = 0.001). The differential profile of gene expression at early and late times in both mutant strains might be caused by the activation of secondary genetic programs and/or changes in the cellular composition of the hippocampus. Thus, in the case of VP16-CREB, we found an enrichment of CREB binding sites in the promoter of upregulated genes at early times after transgene induction (z-test P-value: 0.01), but not at later time (p= 0.13). Interestingly, ~74% of the probe sets significantly altered in the A-CREB late samples were also affected in the VP16-CREB late samples (Fig. 4B-C). This common list, largely made of upregulated probe sets (~96%), revealed changes that were in the same direction in A-CREB and VP16-CREB mice, although their magnitude and statistical significance were consistently larger in VP16-CREB mice (Fig. 4D).

Differential immune response in CREB mutant strains

Enrichment analysis for Gene Ontology (GO) terms showed that genes related with the immune response (complement proteins, chemokines, etc) were overrepresented

among the upregulated genes in both mutant strains (Sup. Fig. S2A). The GO terms *antigen presentation* (containing both MHC class I and II), *production of cytokines, interferon and tumor necrosis factor* and *wounding* were specifically associated to the VP16-CREB late samples. Because of the prominent upregulation of non-neuronal markers related with the immune response in the gene expression profiles of both mutant strains, we evaluated in greater detail the presence of infiltrated immune cells in hippocampal tissue by taking advantage of the publicly available gene expression profiles of several types of immune and glial cells (see Sup. Methods). More than 47 % of the significantly altered probe sets in the A-CREB late samples appeared to have a non-hippocampal origin, and the majority of them were also upregulated in the VP16-CREB^{high} late samples (Fig. 4E). Although these probe sets represented a small proportion of the non-hippocampal probe sets in the VP16-CREB late (~2 %), they ranked among the most prominently changed probe sets (median of the fold-change > 7). Our meta-analysis indicated that most of the non-hippocampal probe sets in the A-CREB late samples could be explained by the presence of macrophage-related cells (Fig. 4F and Sup. Fig. S3A). Interestingly, this analysis revealed three probe sets, corresponding to the *Trat1* and *Alcam* genes, that were strongly upregulated in A-CREB samples, but unaltered in VP16-CREB late samples (see Discussion). In contrast, the presence at late times of non-hippocampal probe sets in the hippocampus of VP16-CREB mice is better explained considering the summation of the molecular signatures of different immune cell types (Fig. 4F and Sup. Fig. S3B). This suggests that a more extensive and specialized immune response and stronger gliosis take place in the hippocampus of VP16-CREB^{high} mice than in that of A-CREB mice. Both histological analyses presented above and qRT-PCR assays for selected genes (Fig. 4G) are in good agreement with these observations.

Comparison with other neurodegenerative processes

To gain new insight into the role of CREB in neurodegenerative processes, we compared the gene expression profiles observed in CREB mutants with those associated with different neurodegenerative conditions in which the deregulation of CREB activity had been previously documented or proposed. This is the case of Huntington's disease (HD) (13, 14, 22), Alzheimer's disease (AD) (15, 23), epilepsy (16, 24) and aging (17, 25-27). Based on some obvious similarities with a recently published gene profiling analysis (28), we extended our comparison to the knockout mouse for palmitoyl-protein thioesterase 1 (PPT1), an animal model for infantile Batten disease (BD). This inheritable disorder, which has not been previously associated to CREB misregulation, is characterized by epilepsy and retinal and cortical neurodegeneration (29).

This meta-analyses revealed limited overlap between the gene profiles of CREB mutants and those of AD and HD mouse models (Fig. 5A). The few genes in common between the AD mouse model and the CREB animals were functionally related with inflammatory responses (Sup. Table 3), whereas in the case of HD mouse models, common changes were primarily associated to the downregulation of neuronal genes, including some potential direct targets of CREB, such as c-*fos* or *Prodynorphin* (Supplemental Table 3 and results not shown). The profile of VP16-CREB-mediated neurodegeneration showed strong correlations with infantile BD and the kainate model of epilepsy (Fig. 5A and Sup. Fig. S4A-C), which encourage further examination of the role of CREB in these pathologies. In contrast, A-CREB profile exhibited very little overlapping with other neurodegenerative profiles, suggesting that dark cell neurodegeneration is a rare in those pathological conditions,

whereas inflammation was much more prevalent. Interestingly, the inspection of the neurodegenerative markers common to several conditions revealed two significantly enriched pathways ($P<0.05$) which correspond to initial steps in the immune responses: the activation of the complement and coagulation cascades, and antigen processing and presentation (Sup. Fig. S4D). These pathways were overrepresented in nearly all the tested conditions, highlighting their relevance in neurodegenerative disorders (Fig. 5B and Sup. Table 3).

DISCUSSION

The picture that emerges from the interdisciplinary analysis of CREB mutants with a loss or a gain-of-function together with previous studies in CREB deficient mice indicates that the precise temporal control of CREB-dependent gene expression is a critical requirement for the viability of CA1 pyramidal neurons and that any imbalance in the activity of this transduction cascade can have a negative impact in the survival and function of these cells, likely through misregulation of their responsiveness to external stimuli, since the electrophysiological alterations preceded the onset of neurodegeneration.

Here, we presented first the ultrastructural signature associated to neurodegeneration induced by chronic inhibition or activation of CREB function. Degenerating neurons in A-CREB mice characteristically exhibited intracellular inclusions, condensation of both the cytoplasm and the nucleus, and ruffling of the plasma membrane, while the ultrastructure of cellular organelles was largely preserved. There was no inflammatory response accompanying neurodegeneration, and as in classical apoptosis, there was minimal damage in the surrounding cells. In contrast, in VP16-CREB mice, we observed a strong activation of astroglia and

microglia as well as other ultrastructural features that suggested an excitotoxic death, in which cellular contents are liberated into the intercellular space damaging neighboring neurons and inducing an inflammatory response. In agreement with these scenarios, the gene profiling analysis showed that the number of markers for inflammation and the magnitude and significance of the changes were higher in VP16-CREB mice than in A-CREB mice and provided interesting cues about the differential evolution of both neurodegenerative processes.

In A-CREB mice, the expression of immune response genes was restricted to some chemokines and components of the complement and phagocytic systems. Interestingly, two immune genes, *Alcam* (Activated leukocyte cell adhesion molecule) and *Trat1* (T-cell receptor interacting molecule or Trim), were strongly upregulated in A-CREB mice and might act as negative modulators of the immune response. Alcam inhibits the transendothelial migration of monocytes (30), thus providing a possible mechanism for limiting the infiltration of immune cells from brain capillaries, whereas Trat1 regulates the surface transport of CTLA-4, an immunoglobulin receptor that dampens T-cell responses (reviewed in (31). Therefore, the increase of Trat1 expression in microglia might limit its activation. These molecules could functionally interact with other negative modulators like the anti-inflammatory Serping1, also called C1 inhibitor, and the autoimmunity suppressor Fc-γIIB (*Fcgr2b*), whose expression is also increased in the hippocampus of A-CREB mice (Sup. Table 1) and could refrain the full activation of the complement pathway and prevent inflammation. In the absence of an inflammatory response, the number of microglia cells might be so low or transient that it escaped our microscopy analysis, but sufficient to increase the expression of innate immune response markers detected

in the gene expression profile, and to clear out apoptotic cells without damaging the surrounding neurons (32) (Fig. 6, right).

In the hippocampus of VP16-CREB^{high} mice, *Alcam* and *Trat1* were not upregulated and the strong activation of microglia (evidenced by the F4/80 marker and the strong up-regulation of *Emr1*) and the complement cascade correlated with a more dramatic cellular response. The over-expression of MHC class I molecules in pyramidal neurons of VP16-CREB^{high} mice (33), maybe physiological in origin (34), might convert them into antigen presenting cells, fuelling the inflammatory process. As a result, we observed glial overactivation (evidenced by the increase in GFAP, aquaporin-4, and other glial markers), the infiltration of peripheral immune cells like T- and B-lymphocytes and dendritic cells, and the release of pro-inflammatory molecules (MHC class II molecules, interleukines, etc) that may work in a positive feed-forward manner (Fig. 6, left).

Our characterization of CREB mutant strains suggests that the strength of complement activation could determine the magnitude and features of the immune response associated to a neurodegenerative process. The two bitransgenic lines described here illustrate two different faces of the immune response in the nervous system: full inflammatory response versus ordered cell death clearance. This view is supported by the EM analysis, the cell death assays and the microarray gene profiling. However, the precise identity of the molecular determinants that separate the role of the complement system in focalized cellular clearance from aggressive inflammation remains undetermined (35). Further use of the analytical approaches described here should define distinctive transcriptional signatures and provide additional clues about the molecular and cellular mechanisms underlying neurodegeneration and maybe reveal novel therapeutic targets.

Finally, these results highlight the perils of prolonged and/or uncontrolled manipulation of the CREB signaling cascade. Although CREB activity has been shown to be neuroprotective in several models of neuronal damage (4, 6, 36-39), it is essential to be careful with the duration and strength of CREB-based therapeutics. In the healthy brain, the phosphorylation of CREB that occurs in response to neuronal activity is transient and promotes the expression of specific downstream genes in a narrow time window. The blockade of this function has dramatic effects in neuronal viability, but the maintenance of strongly elevated levels of CREB activity can be equally devastating.

Acknowledgments: We thank Eva Benito, Eloisa Herrera, Frederic Laumonnier and Jose P. Lopez-Atalaya for critical reading of the manuscript and Roman Olivares for excellent technical assistance. The assistance of Eva Serna and members of the Unidad de Análisis Multigénico at the Facultad de Medicina in the Universidad de Valencia is also acknowledged. The work at AB and LMV lab was supported by the Spanish Ministry of Science and Innovation grants BFU2005-00286, CSD2007-00023 and SAF2008-00611, the Generalitat Valenciana grant GVPRE/2008/365, and the Fundació La Marató de TV3 grant 063510. The work at RL lab was supported by the Spanish Ministry of Science and Innovation grant BFU2006-01896 and the Junta de Comunidades de Castilla-La Mancha grant PAI08-0174-6967.

MATERIALS AND METHODS

Generation and maintenance of transgenic mice

A-CREB (10) and VP16-CREB^{high} (12) mice have been described previously. Both strains have been backcrossed to C57BL/6J for over twenty generations. In all our experiments, we used littermate mice carrying either no transgene or the tTA or *tetO* transgene alone as controls. For VP16-CREB^{high} mice and control littermates doxycyline (dox) was administrated at 40 mg/kg of food and removed to induce transgene expression at the indicated times before experimentation. A-CREB mice were raised without dox. Animal procedures were performed according to the EU and national guidelines for the use of laboratory animals.

Histological techniques

Immunohistochemistry stainings were performed as previously described (11). The following primary antibodies were used: α-cleaved caspase-3 antibodies (Cell Signalling Technology, Beverly, MA), α-VP16 (Santa Cruz Biotechnology Inc., Santa Cruz, CA), α-Flag-M2, α-F4/80 and α-GFAP (Sigma Aldrich Química S.A., Madrid). Secondary biotinylated antibodies, streptividin-peroxidase conjugate, and the DAB substrate were obtained from Sigma and fluorescent secondary antibodies from Invitrogen (Carlsbad, CA). For TUNEL reaction, serial brain sagittal cryosections of 12-µm thickness were stained using the in situ Cell Death Detection Kit (Roche Applied Science, Barcelona, Spain). Silver staining was carried out using the FD Neurosilver^{TM} kit (FD NeuroTechnologies Inc., Catonsville, MD).

Electron microscopy

For electron microscopy mice were anesthetized and perfused with 4% paraformaldehyde and 1% glutaraldehyde in 0.1 M PB (pH 7.4). Then, coronal

sections were cut with a thickness of 60 μm at the level of the dorsal hippocampus using a Leica vibration microtome. After several washes in PB, the sections were postfixed with osmium tetraoxide (1% in 0.1 M PB) and block-stained with uranyl acetate (1% in distilled water). The sections were then dehydrated in ascending series of ethanol to 100% followed by propylene oxide and flat-embedded on glass slides in Durcupan (Fluka, Barcelona). The CA1 region of the hippocampus was cut at 70-90 nm on an ultramicrotome (Reichert Ultracut E; Leica, Austria) and collected on 200-mesh nickel grids. Staining was performed on drops of 1% aqueous uranyl acetate followed by Reynolds's lead citrate. Ultrastructural analyses were performed with a Jeol-1010 electron microscope.

Microarray analysis

For each Mouse Genome 430 2.0 gene expression array (Affymetrix, Santa Clara, CA), total RNA was extracted from the hippocampi of three to four mice with the same age, sex and genotype to produce one pooled sample. We analyzed three late A-CREB pooled samples (six-week old mice) and three late VP16-CREB pooled samples (three-week off dox) with their corresponding control littermate samples (3 pooled samples for each strain). To compare with early changes, we included two pooled A-CREB early samples (three-week old mice) and two pooled VP16-CREB early samples (one-week off dox) with their corresponding control littermate samples. In the case of A-CREB mice, we used the dataset GSE14320 (10). However, in the case of VP16-CREB mice, since earlier gene expression analyses (33) were performed with old MG-U74v2 setA arrays that only interrogated a third of the genome, we prepared new samples from bitransgenic mice and control littermates one week after transgene induction and hybridized them to Mouse Genome 430 2.0 genechips. The new datasets generated in this study will be submitted to the Gene

Expression Omnibus (GEO) database upon manuscript acceptance. The arrays were hybridized, washed and screened for quality according to the manufacturer's protocol. The microarray data was then analyzed using GeneSpring GX 10.0 (Agilent Technologies, Inc., Santa Clara, CA). An RMA algorithm was used for data extraction. Principal component analysis revealed clustering of samples according to the batch of replicates; therefore normalization was conducted using the corresponding control samples values as reference. The filtering criteria were: signal intensities >20% of the maximal expression in all the samples in at least one condition, a fold change >1.5, and $P < 0.05$ in the unpaired Student's t-test. The hierarchical clustering was also performed using GeneSpring software. Additional bioinformatics analyses and the meta-analyses to examine the presence of immune and glial cells markers in the gene expression profiles of CREB mutants and to compare with other neurodegenerative conditions are described in Sup. Methods.

REFERENCES

1. Johannessen M, Delghandi MP, Moens U. What turns CREB on? *Cell Signal* 2004 Nov; **16** (11)**:** 1211-1227.

2. Riccio A, Ahn S, Davenport CM, Blendy JA, Ginty DD. Mediation by a CREB family transcription factor of NGF-dependent survival of sympathetic neurons. *Science* 1999; **286** (5448)**:** 2358-2361.

3. Papadia S, Stevenson P, Hardingham NR, Bading H, Hardingham GE. Nuclear Ca2+ and the cAMP response element-binding protein family mediate a late phase of activity-dependent neuroprotection. *J Neurosci* 2005 Apr 27; **25** (17)**:** 4279-4287.

4. Andreatta CP, Nahreini P, Hanson AJ, Prasad KN. Regulated expression of VP16CREB in neuroblastoma cells: analysis of differentiation and apoptosis. *J Neurosci Res* 2004 Nov 15; **78** (4)**:** 570-579.

5. Glover CP, Heywood DJ, Bienemann AS, Deuschle U, Kew JN, Uney JB. Adenoviral expression of CREB protects neurons from apoptotic and excitotoxic stress. *Neuroreport* 2004 May 19; **15** (7)**:** 1171-1175.

6. Lee B, Butcher GQ, Hoyt KR, Impey S, Obrietan K. Activity-dependent neuroprotection and cAMP response element-binding protein (CREB): kinase coupling, stimulus intensity, and temporal regulation of CREB phosphorylation at serine 133. *J Neurosci* 2005 Feb 2; **25** (5)**:** 1137-1148.

7. Lonze BE, Riccio A, Cohen S, Ginty DD. Apoptosis, axonal growth defects, and degeneration of peripheral neurons in mice lacking CREB. *Neuron* 2002; **34** (3)**:** 371-385.

8. Parlato R, Rieker C, Turiault M, Tronche F, Schutz G. Survival of DA neurons is independent of CREM upregulation in absence of CREB. *Genesis* 2006 Oct; **44** (10)**:** 454-464.

9. Mantamadiotis T, Lemberger T, Bleckmann SC, Kern H, Kretz O, Martin Villalba A*, et al.* Disruption of CREB function in brain leads to neurodegeneration. *Nat Genet* 2002; **31** (1)**:** 47-54.

10. Jancic D, Lopez de Armentia M, Valor LM, Olivares R, Barco A. Inhibition of cAMP Response Element-Binding Protein Reduces Neuronal Excitability and Plasticity, and Triggers Neurodegeneration. *Cereb Cortex* 2009 Feb 12; **19** (11)**:** 2535-2547.

11. Lopez de Armentia M, Jancic D, Olivares R, Alarcon JM, Kandel ER, Barco A. cAMP response element-binding protein-mediated gene expression increases the intrinsic excitability of CA1 pyramidal neurons. *J Neurosci* 2007 Dec 12; **27** (50)**:** 13909-13918.

12. Barco A, Alarcon JM, Kandel ER. Expression of constitutively active CREB protein facilitates the late phase of long-term potentiation by enhancing synaptic capture. *Cell* 2002 Mar 8; **108** (5)**:** 689-703.

13. Shimohata T, Nakajima T, Yamada M, Uchida C, Onodera O, Naruse S*, et al.* Expanded polyglutamine stretches interact with TAFII130, interfering with CREB-dependent transcription. *Nat Genet* 2000 Sep; **26** (1)**:** 29-36.

14. Sugars KL, Brown R, Cook LJ, Swartz J, Rubinsztein DC. Decreased cAMP response element-mediated transcription: an early event in exon 1 and full-length cell models of Huntington's disease that contributes to polyglutamine pathogenesis. *J Biol Chem* 2004 Feb 6; **279** (6)**:** 4988-4999.

15. Vitolo OV, Sant'Angelo A, Costanzo V, Battaglia F, Arancio O, Shelanski M. Amyloid beta -peptide inhibition of the PKA/CREB pathway and long-term potentiation: reversibility by drugs that enhance cAMP signaling. *Proc Natl Acad Sci U S A* 2002 Oct 1; **99** (20)**:** 13217-13221.

16. Park SA, Kim TS, Choi KS, Park HJ, Heo K, Lee BI. Chronic activation of CREB and p90RSK in human epileptic hippocampus. *Exp Mol Med* 2003 Oct 31; **35** (5)**:** 365-370.

17. Bach ME, Barad M, Son H, Zhuo M, Lu YF, Shih R*, et al.* Age-related defects in spatial memory are correlated with defects in the late phase of hippocampal long-term potentiation in vitro and are attenuated by drugs that enhance the cAMP signaling pathway. *Proc Natl Acad Sci U S A* 1999; **96** (9)**:** 5280-5285.

18. Lonze BE, Ginty DD. Function and regulation of CREB family transcription factors in the nervous system. *Neuron* 2002 Aug 15; **35** (4)**:** 605-623.

19. Turmaine M, Raza A, Mahal A, Mangiarini L, Bates GP, Davies SW. Nonapoptotic neurodegeneration in a transgenic mouse model of Huntington's disease. *Proc Natl Acad Sci U S A* 2000 Jul 5; **97** (14)**:** 8093-8097.

20. Leist M, Jaattela M. Four deaths and a funeral: from caspases to alternative mechanisms. *Nat Rev Mol Cell Biol* 2001 Aug; **2** (8)**:** 589-598.

21. Ishimaru MJ, Ikonomidou C, Tenkova TI, Der TC, Dikranian K, Sesma MA*, et al.* Distinguishing excitotoxic from apoptotic neurodegeneration in the developing rat brain. *J Comp Neurol* 1999 Jun 14; **408** (4)**:** 461-476.

22. Shimohata M, Shimohata T, Igarashi S, Naruse S, Tsuji S. Interference of CREB-dependent transcriptional activation by expanded polyglutamine stretches--augmentation of transcriptional activation as a potential therapeutic strategy for polyglutamine diseases. *J Neurochem* 2005 May; **93** (3)**:** 654-663.

23. Gong B, Vitolo OV, Trinchese F, Liu S, Shelanski M, Arancio O. Persistent improvement in synaptic and cognitive functions in an Alzheimer mouse model after rolipram treatment. *J Clin Invest* 2004 Dec; **114** (11)**:** 1624-1634.

24. Brooks-Kayal AR, Raol YH, Russek SJ. Alteration of epileptogenesis genes. *Neurotherapeutics* 2009 Apr; **6** (2)**:** 312-318.

25. Brightwell JJ, Gallagher M, Colombo PJ. Hippocampal CREB1 but not CREB2 is decreased in aged rats with spatial memory impairments. *Neurobiol Learn Mem* 2004 Jan; **81** (1)**:** 19-26.

26. Tomobe K, Okuma Y, Nomura Y. Impairment of CREB phosphorylation in the hippocampal CA1 region of the senescence-accelerated mouse (SAM) P8. *Brain Res* 2007 Apr 13; **1141:** 214-217.

27. Porte Y, Buhot MC, Mons N. Alteration of CREB phosphorylation and spatial memory deficits in aged 129T2/Sv mice. *Neurobiology of aging* 2008 Oct; **29** (10)**:** 1533-1546.

28. Qiao X, Lu JY, Hofmann SL. Gene expression profiling in a mouse model of infantile neuronal ceroid lipofuscinosis reveals upregulation of immediate early genes and mediators of the inflammatory response. *BMC neuroscience* 2007; **8:** 95.

29. Haltia M. The neuronal ceroid-lipofuscinoses: from past to present. *Biochim Biophys Acta* 2006 Oct; **1762** (10)**:** 850-856.

30. Masedunskas A, King JA, Tan F, Cochran R, Stevens T, Sviridov D*, et al.* Activated leukocyte cell adhesion molecule is a component of the endothelial junction involved in transendothelial monocyte migration. *FEBS Lett* 2006 May 15; **580** (11)**:** 2637-2645.

31. Rudd CE, Taylor A, Schneider H. CD28 and CTLA-4 coreceptor expression and signal transduction. *Immunol Rev* 2009 May; **229** (1)**:** 12-26.

32. Bonifati DM, Kishore U. Role of complement in neurodegeneration and neuroinflammation. *Mol Immunol* 2007 Feb; **44** (5)**:** 999-1010.

33. Barco A, Patterson S, Alarcon JM, Gromova P, Mata-Roig M, Morozov A*, et al.* Gene Expression Profiling of Facilitated L-LTP in VP16-CREB Mice Reveals that BDNF Is Critical for the Maintenance of LTP and Its Synaptic Capture. *Neuron* 2005 Oct 6; **48** (1)**:** 123-137.

34. Huh GS, Boulanger LM, Du H, Riquelme PA, Brotz TM, Shatz CJ. Functional requirement for class I MHC in CNS development and plasticity. *Science* 2000; **290** (5499)**:** 2155-2159.

35. Alexander JJ, Anderson AJ, Barnum SR, Stevens B, Tenner AJ. The complement cascade: Yin-Yang in neuroinflammation--neuro-protection and -degeneration. *J Neurochem* 2008 Dec; **107** (5)**:** 1169-1187.

36. Gao Y, Deng K, Hou J, Bryson JB, Barco A, Nikulina E*, et al.* Activated CREB Is Sufficient to Overcome Inhibitors in Myelin and Promote Spinal Axon Regeneration In Vivo. *Neuron* 2004 Nov 18; **44** (4)**:** 609-621.

37. Deng W, Neve RL, Rosenberg PA, Volpe JJ, Jensen FE. AMPA receptor subunit composition and CREB regulate oligodendrocyte excitotoxicity. *J Biol Chem* 2006 Sep 21; **281** (47)**:** 36004-36011.

38. Kitagawa K. CREB and cAMP response element-mediated gene expression in the ischemic brain. *FEBS J* 2007 Jul; **274** (13)**:** 3210-3217.

39. Choi YS, Lee B, Cho HY, Reyes IB, Pu XA, Saido TC*, et al.* CREB is a key regulator of striatal vulnerability in chemical and genetic models of Huntington's Disease. *Neurobiol Dis* 2009 Jul 23; **36** (2)**:** 256-268.

40. Viosca J, Malleret G, Bourtchouladze R, Benito E, Vronskava S, Kandel ER*, et al.* Chronic enhancement of CREB activity in the hippocampus interferes with the retrieval of spatial information. *Learn Mem* 2009; **16** (3)**:** 198-209.

Figure legends

Figure 1. Death of A-CREB expressing neurons. Electron micrographs of pyramidal neurons in the CA1 subfield of the dorsal hippocampus of A-CREB mice. **A.** Micrographs of the CA1 subfield in a control mouse. **B-C.** Micrographs of the CA1 subfield in six-week old A-CREB mice reveal the presence of heteropycnotic pyramidal cells (black arrows in Panel **B,** quantification in bar graph inset) not observed in sections from control littermates. Heteropycnotic neurons showed early signs of apoptotic-like degeneration, consisting of cell bodies markedly reduced in size and increased electron density as a result of mild condensation of the nucleus and the cytoplasm, and morphologically injured mitochondria. The inset in panel **C** shows a higher magnification image of the convoluted nuclear membrane and the chromatin clumps around the inner membrane of the nucleus (white arrows). Scale: A = 20 microns; C = 6 microns. **D.** Representative images of TUNEL reaction in the hippocampus of six- and eight-week old A-CREB mice (AC) and control littermates (WT). Three control and four mutant mice (two per time point) were analyzed. Scale: 70 μm.

Figure 2. Death of VP16-CREB expressing neurons. A. Electron micrographs of pyramidal neurons in the CA1 subfield of the dorsal hippocampus of VP16-CREB^{high} mice showing progressive neurodegeneration after transgene induction. Micrographs of the CA1 subfield in control littermates (**A**) were undistinguishable of those of VP16-CREB^{high} one or two weeks after transgene induction. Three weeks after transgene induction, a number of ultrastructural changes were appreciable both in the cellular layer (**B** and **D**, the left inset in Panel D shows a higher magnification image of the framed area) and the *stratum radiatum*. Six weeks after transgene expression the disorganization of the hippocampus was evident (**C**) and a large number of glial

cells were found in the *stratum radiatum* and in the proximity of pyramidal cell bodies, in some cases, phagocytosing those cells (**E**). Abbreviations: sr, *stratum radiatum*; so, *stratum oriens*. Asterisk, glial cell process; black arrow, glial cell nucleus. Scale bars: A-C = 5 microns; D-E = 2 microns. **F-L:** Electron microscopy of synapses in the stratum radiatum of VP16-CREB mice. Micrographs in control littermates (**F** and **H**) were undistinguishable of those of VP16-CREB^{high} one (results not shown) or two weeks after transgene induction (**G** and **I**). Both inhibitory (**F**-**G**) and excitatory synapses (**H-I**) were normal. In contrast, three weeks after transgene induction, a number of ultrastructural changes were appreciable in both inhibitory (**J**) and excitatory (**K**) synapses. Six weeks after transgene expression (**L**), the disorganization of the *stratum radiatum* was profound. Abbreviations: Py, pyramidal cell; bt, basket cell terminal; s, spine; b, button or axon terminal; Den, dendritic shaft; ax, axons; G, glial cell process. Scale bars : 0.5 microns. **M.** Quantification of the number of excitatory synapses at different time points after transgene induction. **N.** Representative images of TUNEL reaction (green) in the hippocampus of VP16-CREB^{high} mice and control littermates three weeks after transgene induction (n=3 for both genotypes). Sections were counterstained with DAPI (blue). Scale: 50 μm.

Figure 3. Gliosis in VP16-CREB^{high} mice. A. Left, GFAP immunostaining of the hippocampus of VP16-CREB^{high} mice expressing (On, three weeks after transgene induction) or not expressing the transgene (Off, animals fed with dox food). Sections were double stained with antibodies against GFAP (red) and VP16 (green) and counterstained with DAPI (blue). Right, GFAP immunostaining of the hippocampus of six-week old A-CREB mice. Sections were double stained with antibodies against GFAP (red) and Flag-M2, which recognizes A-CREB (green), and counterstained with DAPI (blue). The right insets show higher magnification images. At least 3

independent mice per condition were used in this analysis. **B.** Immunostaining using antibodies against the microglia marker F4/80 revealed the presence of reactive microglia only in the hippocampus of VP16-CREB^{high} mice (white arrows in higher magnification insets), whereas A-CREB mice did not show enhanced signal for this marker. Three bitransgenic mice and three control littermates were used in this comparison. Scale bars: 140 μm.

Figure 4. **Comparison of gene expression profiles in the hippocampus of A-CREB and VP16-CREB^{high} mice. A.** The percentage of upregulated (black) and downregulated (white) probe sets at early and late times, as well as the number of probe sets altered in each condition (number on the right side), is shown. **B.** Squared-Euclidean hierarchical clustering of the significantly altered probe sets in both bitransgenic hippocampi. Red, upregulation; yellow, no change; blue, downregulation. **C.** Venn diagram presenting the total number of affected probe sets and the overlap in the profiles of A-CREB and VP16-CREB late samples. **D.** Graphs showing the median of the fold changes (left) as a measure of the magnitude of the changes, and the median of the *P*-values (right) as a measure of their significance. 'Specific' (white bars) refers to probe sets that passed the filters in only one of the two bitransgenic strains, whereas 'Common' (gray bars) passed in both strains. **E.** Percentage of non-hippocampal probe sets (left) and median of the fold change (right) in either A-CREB or VP16-CREB^{high} late samples (white bars), and common to both strains (gray bars). The number of probe sets is indicated above each bar. **F.** Percentage of non-hippocampal genes and associated cell types: macrophages and microglia (green), dendritic and mast cells (red), glial cells (yellow), and others (blue). The numbers represent the number of genes for each cell group (see Sup. Fig. 3 for additional detail). **G.** qRT-PCR assays for selected genes and comparison with

the fold change of the corresponding probe sets in the microarray analysis. *, $P<0.05$; **, $P<0.01$ Student's t test.

Figure 5. Meta-analysis of neuropathological models. A. Correlation analysis of the transcriptional alterations associated to each on of the following pathological conditions: mouse model of AD (Presenilin conditional double knockout), aging (24 months old animals), kainate-induced epilepsy (10 d after injection), HD (R6/1, R6/2, and CHL2), Batten disease (PPT1 8 months old knockout), and A-CREB and VP16-CREB^{high} mice at late times after transgene expression. See coloring legend for coefficient values. The percentage of altered genes common to the late expression profiles of VP16-CREB^{high} mice and A-CREB mice is indicated in the right table. 'Up' and 'Down' distinguish between upregulated and downregulated genes, respectively. **B.** Significative enrichment for canonical KEGG pathways reveals the presence of complement and antigen presentation genes in the profiles of neurodegenerative models. Analysis was performed using genes present at least in three (>2 common, white bars) or four (>3 common, black bars) (P-value < 0.05, see Supplemental Materials).

Figure 6. Bidirectional control of CA1 neuronal survival and plasticity by CREB. Summary of opposite and coincidental alterations detected during the multidisciplinary characterization of transgenic strains with regulatable enhancement or inhibition of CREB function (references are indicated with numbers). The bottom drawings show heuristic models for the cell death mechanisms activated in each mouse strain according to the results of the ultrastructural and transcriptional profiling. [a] (12, 33); [b] (12) and others; [c] (11) and others; [d] (10, 11); [e] (40) and others; [f] (10) and others.

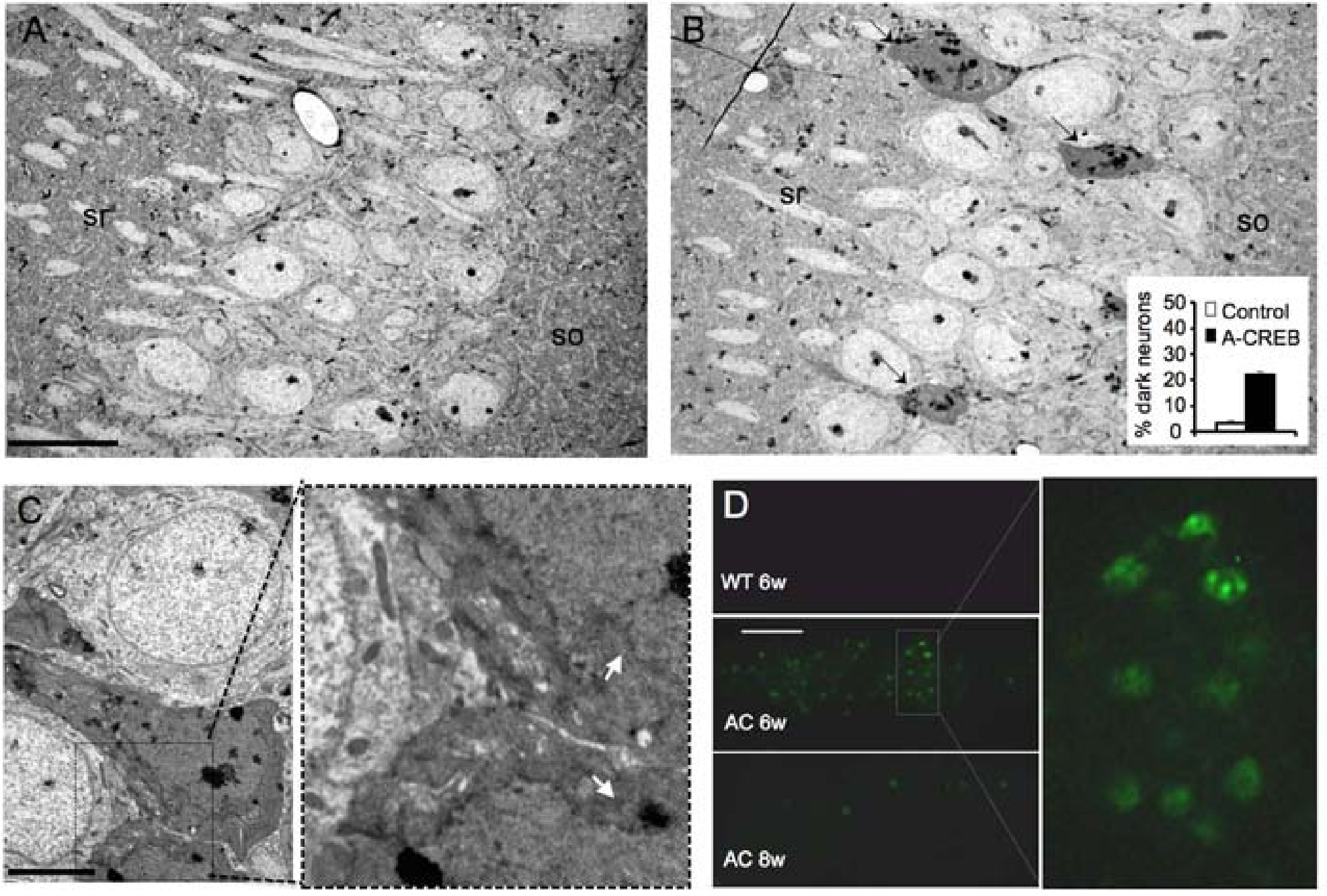
A
sr
so
B
sr
so
% dark neurons
50
40
30
20
10
0
Control
A-CREB
C
D
WT 6w
AC 6w
AC 8w

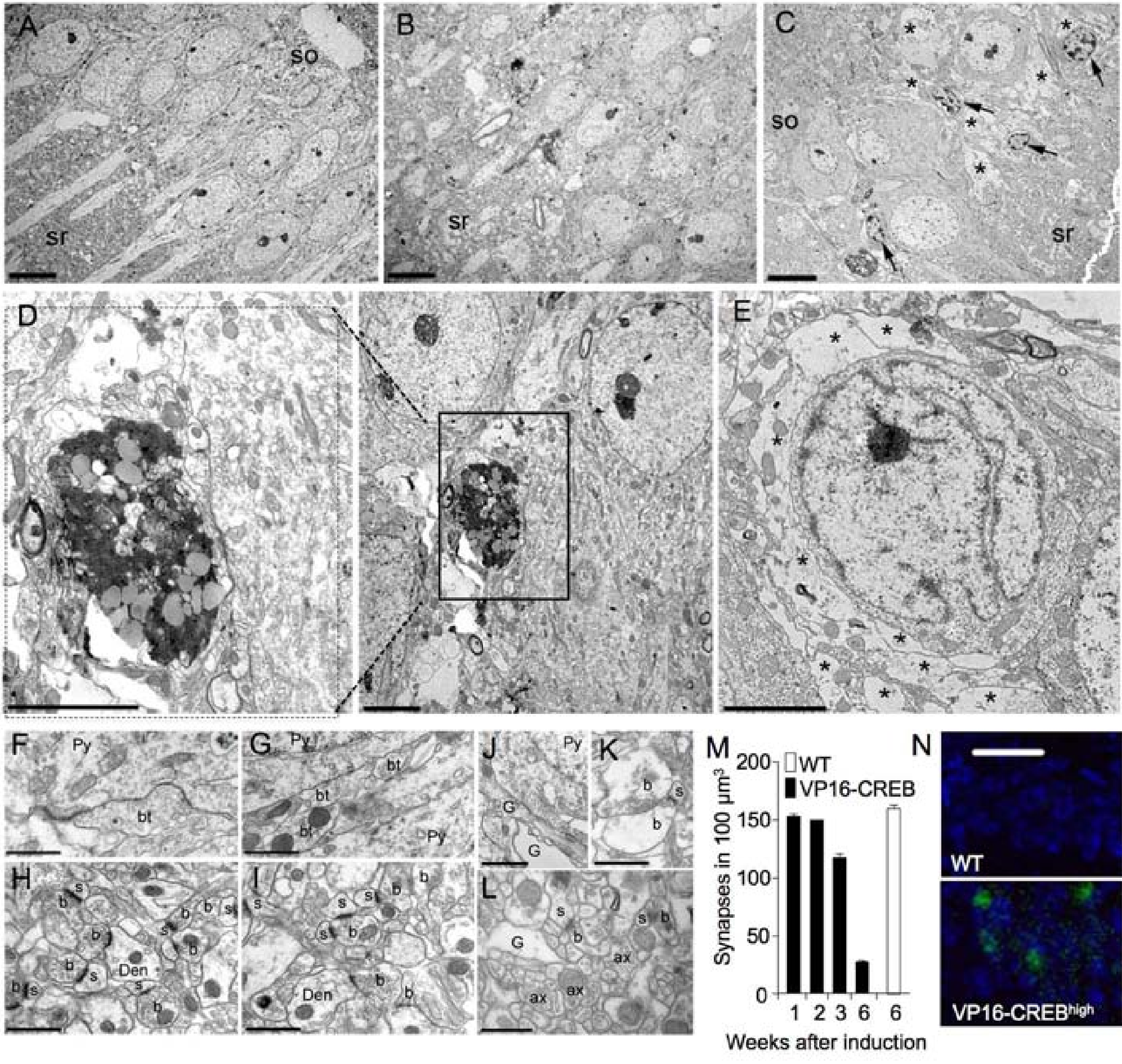
A
so
sr
B
sr
C
so
sr
D
E
F
Py
bt
G
Py
bt
bt
Py
J
Py
G
G
K
b
s
b
H
b
s
b
b
b
s
b
b
b
s
b
Den
s
b
s
b
b
I
s
b
b
s
s
s
b
b
Den
b
b
L
s
s
b
s
b
G
b
ax
ax
ax
M
Synapses in 100 µm³
200
150
100
50
0
WT
VP16-CREB
1 2 3 6 6
Weeks after induction
N
WT
VP16-CREB^high

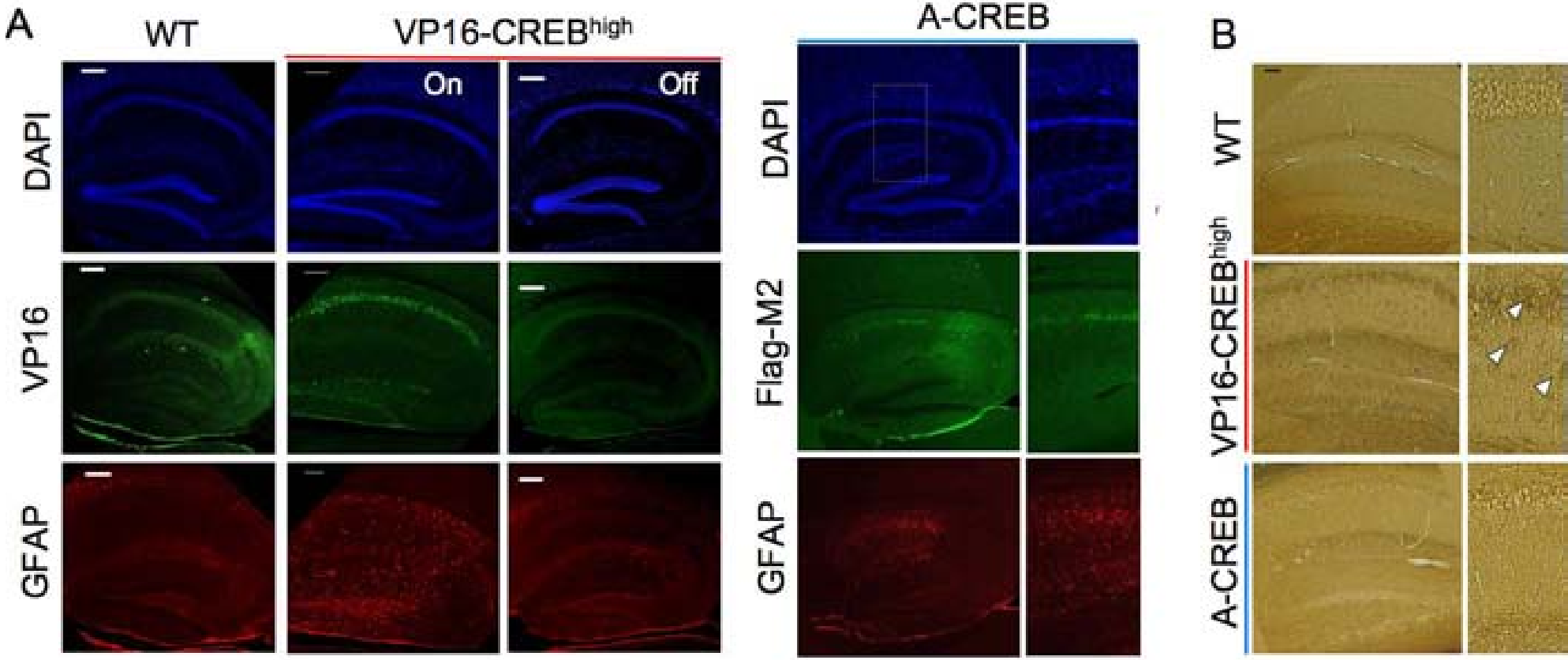
A
WT
VP16-CREB^high
On
Off
A-CREB
DAPI
VP16
GFAP
DAPI
Flag-M2
GFAP
B
WT
VP16-CREB^high
A-CREB

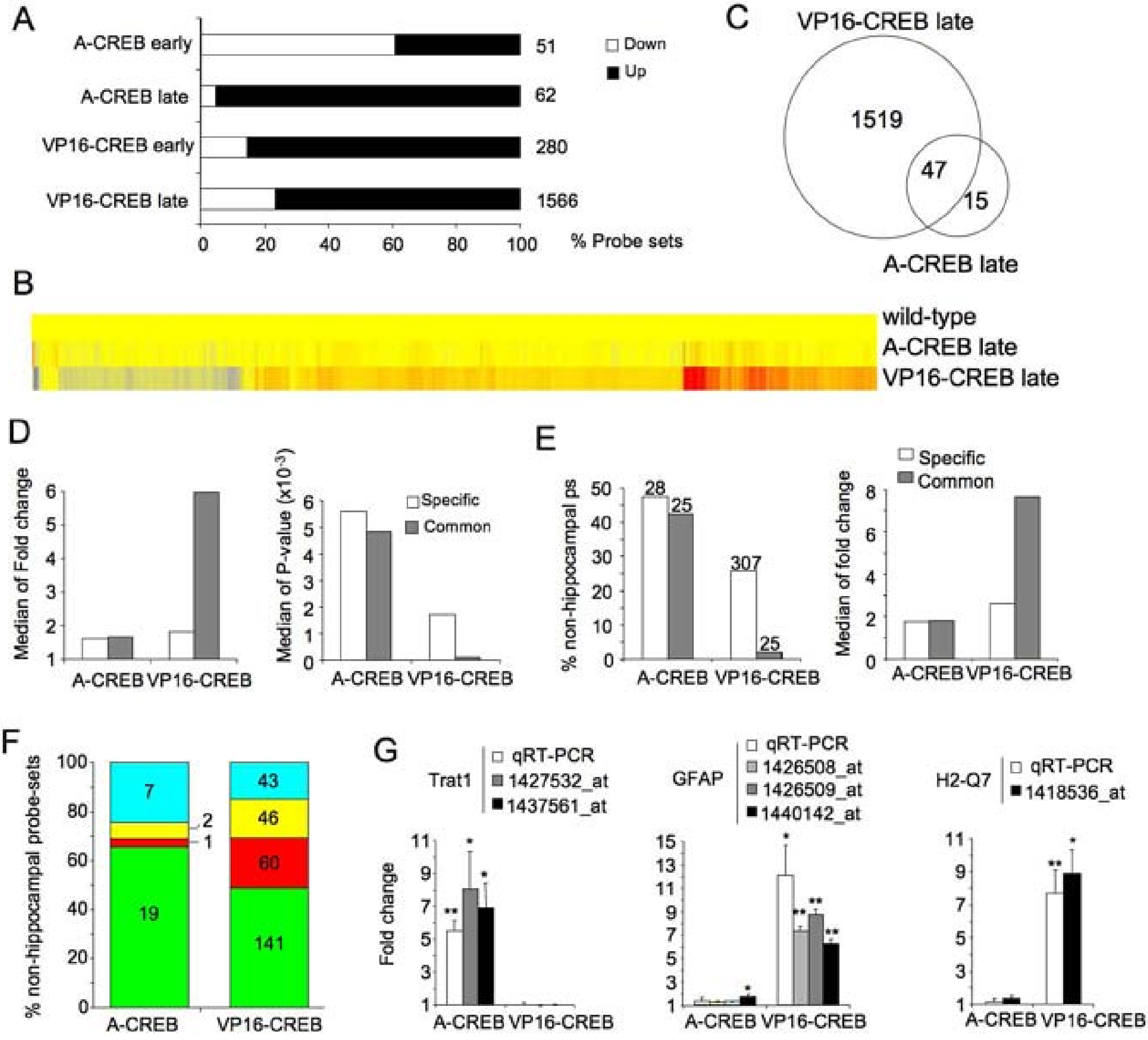
A
A-CREB early
A-CREB late
VP16-CREB early
VP16-CREB late
51
62
280
1566
Down
Up
0
20
40
60
80
100
% Probe sets
C
VP16-CREB late
1519
47
15
A-CREB late
B
wild-type
A-CREB late
VP16-CREB late
D
Median of Fold change
A-CREB
VP16-CREB
Median of P-value (x10-3)
Specific
Common
E
% non-hippocampal ps
28
25
307
25
Median of fold change
F
% non-hippocampal probe-sets
7
2
1
19
43
46
60
141
G
Trat1
qRT-PCR
1427532_at
1437561_at
Fold change
GFAP
1426508_at
1426509_at
1440142_at
H2-Q7
1418536_at

A

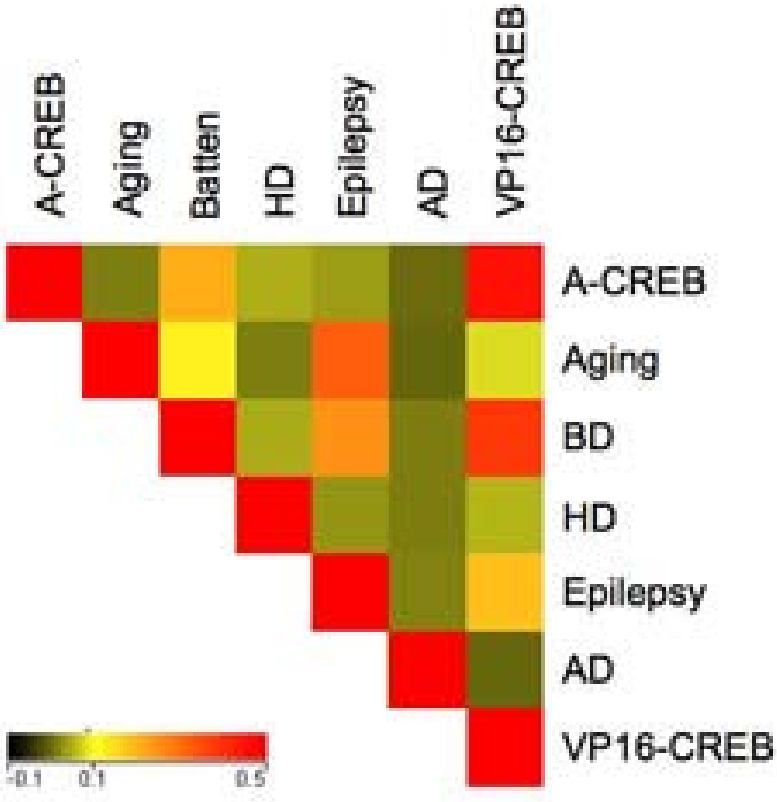

VP16-CREB	Up	Down	A-CREB
75%	76%	67%	100%
40%	45%	0%	6%
37%	59%	7%	3%
13%	13%	13%	1%
74%	75%	50%	8%
7%	10%	2%	1%
100%	100%	100%	4%

B

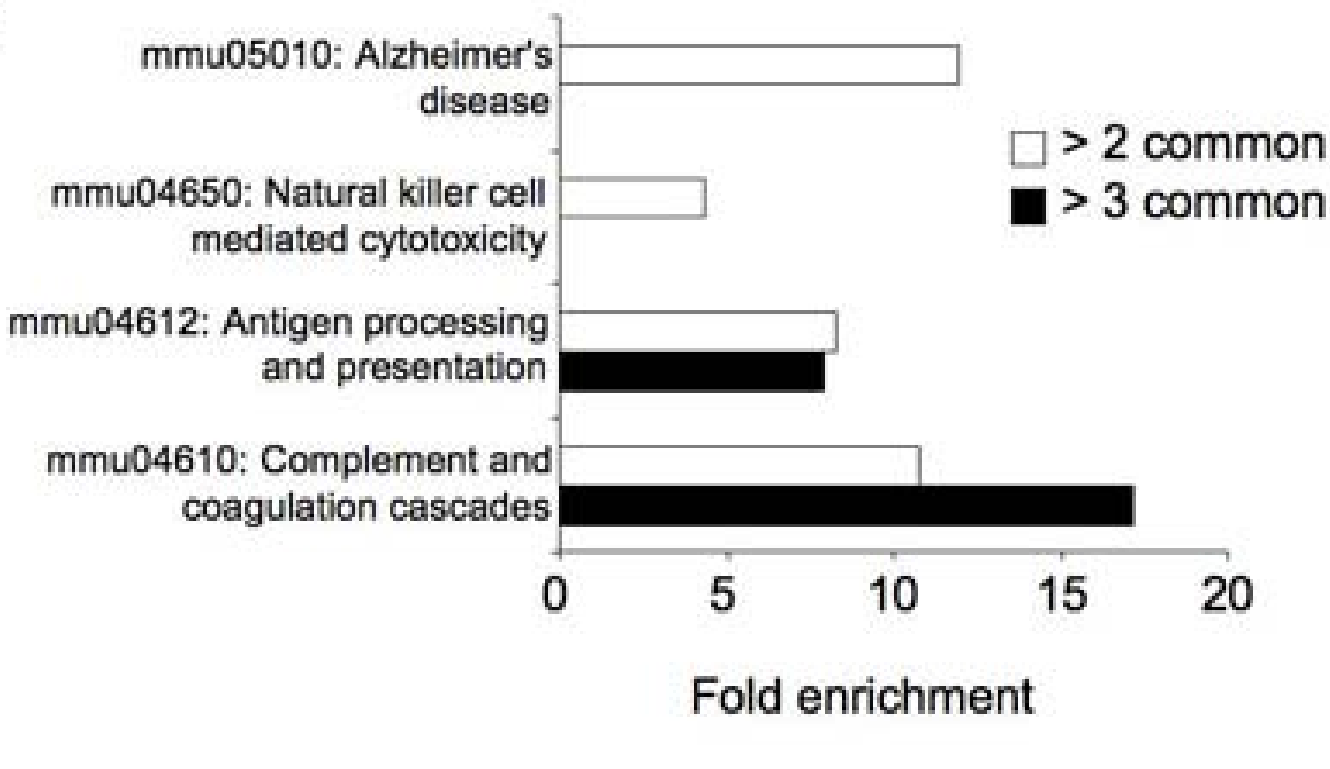

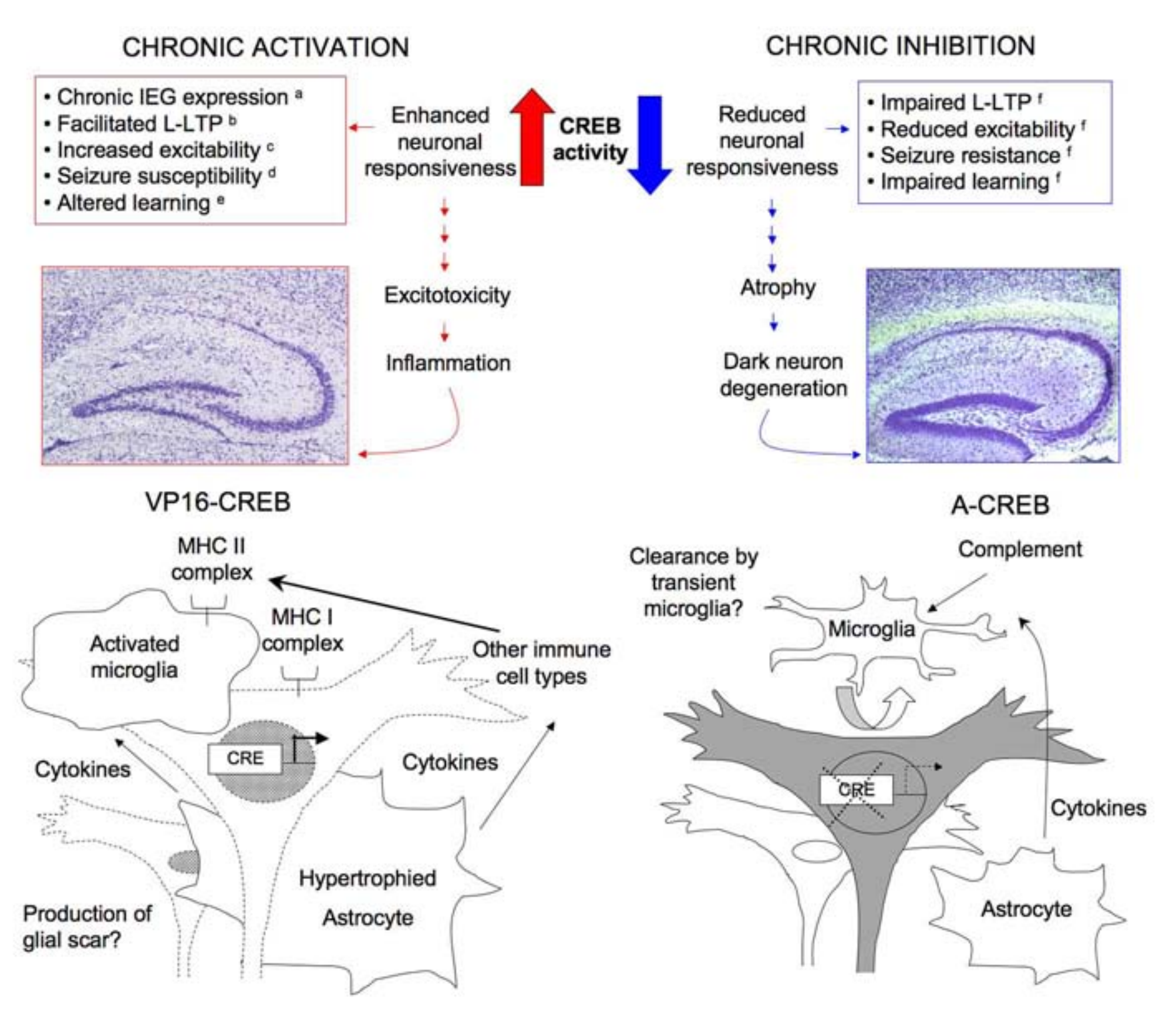
CHRONIC ACTIVATION
CHRONIC INHIBITION
• Chronic IEG expression [a]
• Facilitated L-LTP [b]
• Increased excitability [c]
• Seizure susceptibility [d]
• Altered learning [e]
Enhanced neuronal responsiveness
CREB activity
Reduced neuronal responsiveness
• Impaired L-LTP [f]
• Reduced excitability [f]
• Seizure resistance [f]
• Impaired learning [f]
Excitotoxicity
Inflammation
Atrophy
Dark neuron degeneration
VP16-CREB
A-CREB
MHC II complex
MHC I complex
Activated microglia
Other immune cell types
CRE
Cytokines
Cytokines
Hypertrophied Astrocyte
Production of glial scar?
Clearance by transient microglia?
Complement
Microglia
CRE
Cytokines
Astrocyte